Candidate Proof Mass Actuator Control Laws for the Vibration Suppression of a Frame

Jeffrey W. Umland†

Daniel J. Inman††

Dept. of Mechanical and Aerospace Engineering
University at Buffalo
Buffalo, NY 14260

Abstract

The vibration of an experimental flexible space truss is controlled with internal control forces produced by several proof mass actuators. Four candidate control law strategies are evaluated in terms of performance and robustness. These control laws are experimentally implemented on a quasi free-free planar truss. Sensor and actuator dynamics are included in the model such that the final closed loop system is self-equilibrated. The first two control laws considered are based on direct output feedback and consist of tuning the actuator feedback gains to the lowest mode intended to receive damping. The first method feeds back only the proof mass's position and velocity relative to the structure, this results in a traditional vibration absorber. The second method includes the same feedback paths as the first plus feedback of the local structural velocity. The third control law is designed with robust H_∞ control theory. The fourth control strategy is an active implementation of a viscous damper, where the actuator is configured to provide a bending moment at two points on the structure.

The vibration control system is then evaluated in terms of how it would benefit the space structure's position control system. This assessment is necessary since the additional actuator dynamics in the model effectively adds two state variables to the system which could lead to instabilities in the position control system.

1 Introduction

Proof mass actuators (PMA's) have been considered for use in large space structure vibration control systems[1]. These control systems are usually configured such that the PMA's provide a closed loop control force based on the output from a combination of both colocated and noncolocated sensors[2,3]. The colocated sensor provides measurements of the position of the proof mass relative to the structure. A benefit of colocated control is that stable control laws can be designed that provide vibration attenuation at the point of actuator attachment. Several experimental implementations of colocated PMA control have resulted in control laws that are based on the traditional vibration absorber[4,5]. In an effort to gain increased vibration attenuation, noncolocated sensors provide actual structural vibration measurements at the point where performance is desired. The problem of designing a noncolocated control is constrained by the requirement that the control law must provide stable vibration suppression at sensor locations on a flexible structure that is not necessarily well modeled.

This paper addresses the issue of the effective use of the proof mass actuator's control effort towards the robust vibration suppression of a flexible unconstrained planar frame. An

† Graduate Research Assistant
†† Professor

unconstrained or free-free structure is used, rather than a constrained or cantilevered structure. It is observed that in some cases an entire vehicle will vibrate indicating that a constrained analysis is not appropriate[7,8]. The approach taken is to compare several control law and actuator-sensor combinations when the actuator provides a point force on the structure. As a counterpoint, the actuator is also mounted to the structure such that the actuator's control effort provides both an axial force and a bending moment applied at two points on the structure. A control structure interaction approach is undertaken in the sense that the actuator, sensor, and controller dynamics are included or accounted for in the structural control design.

The paper outline is as follows: Section 1 gives an introduction to the control structure interaction problem undertaken here. The flexible structure control testbed is described in Section 2. The PMA control law designs to be compared are detailed in Section 3. The results of experimental implementation of these control laws are provided in Section 4. The research is summarized in the final section.

2 Hardware Description

The experimental flexible structure is constructed such that it exhibits the characteristics commonly associated with large flexible space structures. The structure is light weight, with most of its mass concentrated at the joints. There are both colocated and noncolocated sensors and actuators. The structure displays numerous modes of vibration that have a low natural frequency, are lightly damped, and are closely spaced relative to each other. A soft cable suspension system is used to simulate the free boundary conditions of space, and to minimize the effects of attaching the structure to ground.

2.1 Flexible Structure

Figure 1 illustrates the 6-bay, 3 m long plane frame. The width of the structure is 0.5 m, and the diagonal dimension is 0.707 m. The frame is constructed from aluminum truss links and joints manufactured by the Mero Corporation. A truss link consists of an aluminum tube, with nominal cross section dimensions of 22 mm O. D. and 20 mm I. D., terminated in bolt assemblies which attach to the truss nodes. The truss node is Mero's standard M12 aluminum node. The links are attached to the nodes and tightened with a torque wrench to 25 in-lb. The total weight of the structure is 61 N.

The frame is suspended from the ceiling by two soft bungee cables 2 m in length. It was found necessary to double up the cables to support the total weight of the structure and actuators. The cables are attached at nodes 2 and 6. These joints were chosen for the suspension points since they were nearly coincident with the nodes of the first structural mode of vibration, therefore minimizing the interaction of the structure and its suspension. The electrical cables are suspended from the ceiling such that they do not carry the weight of the structure, and the mass loading of the structure by these cables is minimized.

The dynamic characteristics of this structure are evident in figure 2, which shows an experimental transfer function of node 1's linear acceleration in the x direction given an impact at node 1 in the x direction. The modal properties of the first 8 structural modes of vibration are given in table 1. The vibration of the frame is characterized by flexural deflection rather than axial deflection that would occur in a true truss structure. The structure is sufficiently long such that the low structural vibration modes are not coupled to local member bending modes.

Not all of the dynamic characteristics displayed in figure 2 can be attributed to the structure, rather the suspension provides a significant portion of the response shown in this test. Three pendulous modes at approximately 1/3 Hz replaced the three rigid body modes in the x-y plane. A double pendulum mode at 1.2 Hz replaced the rigid body rotation about the y -axis. Translation in the z direction and rotation about the x axis are replaced by two translational vibration modes at 1/2 Hz which are due to stretching of the suspension cables. The cables also have transverse vibration modes that occur at 12 Hz, 37 Hz, and 55 Hz.

2.1.1 Structural Model

A finite element model of the structure was constructed for use in control design. The frame links were modeled as uniform aluminum tubes whose dimensions are the same as the manufacturer's nominal specifications. The frame joints were modeled as rigid. The combined mass of the joints and the link bolt assemblies were modeled as a point mass, with zero rotational inertia, located at each finite element node. Table 2 gives the structural parameters used in the finite element analysis. In order to simplify the model, Guyan reduction was used to eliminate translation in both the z and y directions, and rotations about the x axis. Only motion out of the y-z plane is modeled.

The transverse vibration of the suspension cables was also modeled, since these vibration modes appear in the control bandwidth. Modeling the suspension gave better agreement between the pole-zero pairs as shown in figure 2.

2.2 Proof Mass Actuators

The proof mass actuators used are illustrated in figure 3. These actuators were originally developed at the NASA Langley Research Center[1]. The intent of this design is that a magnetic field is produced by the permanent magnets and the iron in the proof mass that is normal to the current flowing through conductors in the coil. This electromagnetic coupling is then described by Eq. 1.

$$\mathbf{F} = nl\mathbf{I} \times \mathbf{B} \tag{1}$$

I represents the current carried in the conductor, n the number of conductors in the gap, **B** the magnetic field across the gap, l the length of the conductor. An average conductor length is found from the average circumference around the coil. A useful control force oriented along the axis of the coil results from this coupling. This force is then applied to the conductors in the coil, and subsequently the structure. The reaction of this force is applied to the proof mass and causes it to translate upon a linear bearing. Hence, the PMA can be modeled as providing an ideal point force at the place of attachment on the structure and a reaction force on the proof mass. This force is taken to be proportional to the current supplied to the coil. The power amplifier for the actuator is configured as a current amplifier, which provides a means by which the actuator can be controlled by a voltage signal. The proof mass actuator characteristics are given in table 3.

A complete model of the PMA should also include the dead mass and rotational inertia associated with the actuator. The motivation behind this is that for lightweight structures the actuator's dead mass will constitute a significant percentage of the total mass of the structure. The addition of a relatively large discrete mass to a structure has the tendency to attract the nodes of the higher modes of vibration of the structure to the point of attachment. This effect minimizes the ability of a point force to provide a useful control force to higher modes of vibration. The rotational inertia of the actuator used here cannot be considered negligible compared to the structure. The high actuator inertia is in part due to the overall length of actuator measured from the base.

2.2.1 Actuator Nonlinearities

There are several nonlinearities associated with the actuator, several of these are better described as saturation limits. The total stroke length of the proof mass is ±0.0127 m. The actuator produces a useful control force only when the proof mass is free to translate. Therefore, feedback of the proof mass position relative to the structure is used to maintain the proof mass in

the center of its stroke. The finite stroke length is the limiting factor for low frequency, large amplitude motions.

The power amplifier used is operated as a voltage controlled current amplifier On the amplifier there is a current limiter that provides for a saturation limit on the output. The maximum output current of the amplifier determines the maximum force output of the actuator. An important design tradeoff here is to determine how much control effort should be used towards the proof mass centering force and how much should be available for a control force based on a noncolocated sensor.

The damping in the actuator is primarily due to friction in the linear bearing and steel shaft interface. This friction has been described by a typical Coulomb friction relation. The normal load that generates the friction force is a combination of the weight of the proof mass and a magnetic force between the permanent magnets and the steel shaft and ball bearings. These frictional effects further limit the effectiveness of the actuator at low frequencies. Secondly, the source of the damping is important in the sense that previously implemented PMA control laws have relied upon available actuator damping to obtain closed loop stability. The problem is that a large portion of this damping would not be available in a zero-g environment.

The electromagnetic coupling between the coil and the proof mass is described by Eq. 1 for only a portion of the total stroke. This is illustrated in figure 4. This plot shows the static force produced by the actuator for a constant input current. Ideally the actuator should output a constant force for a constant input current independent of the stroke position. During bench testing of the actuator, this led to closed loop instability.

2.2.2 Attachment to Structure

The structural equations of motion must be modified to include the actuator dynamics. The structure is originally described by m degrees of freedom $\mathbf{x}$, and if n actuators are used then n degrees of freedom represented by the relative displacements η are appended to the equations of motion. Note that the coupling appears in the mass matrix rather than the stiffness matrix.

$$M_{ol}\,\ddot{\mathbf{x}} + K_{ol}\,\mathbf{x} = B\,\mathbf{f_g} \tag{2a}$$

$$\mathbf{x} = \left\{ x_{fem} \quad \eta_{act} \right\}^T \tag{2b}$$

$$K_{ol} = \begin{bmatrix} K_{fem} & 0_{mxn} \\ 0_{nxm} & 0_{nxn} \end{bmatrix} \tag{2c}$$

$$M_{ol} = \begin{bmatrix} M_{fem} & 0_{mxn} \\ 0_{nxm} & 0_{nxn} \end{bmatrix} + \begin{bmatrix} M_d + J_d + M_{p1} & M_{p2} \\ M_{p2}^T & m_p I_{nxn} \end{bmatrix} \tag{2d}$$

$$M_d = m_d\ \mathrm{diag}(0,\ldots,\ 0,1,0,0,\ldots,0) \tag{2e}$$

$$J_d = j_d\ \mathrm{diag}(0,\ldots,\ 0,0,1,0,\ldots,0) \tag{2f}$$

$$M_{p1} = m_p\ \mathrm{diag}(0,\ldots,\ 0,1,0,0,\ldots,0) \tag{2g}$$

$$M_{p2j} = m_p(0,\ldots,\ 0,1,0,0,\ldots,0)^T,\ j = 1{:}n \tag{2h}$$

$$B = \begin{bmatrix} 0_{mxn} \\ g_{act} I_{nxn} \end{bmatrix} \tag{2i}$$

2.3 Linear Variable Differential Transformer

A linear variable differential transformer (LVDT) is mounted on each PMA to provide a measurement of the proof mass position relative to the structure. The LVDT used is a Schaevitz Eng. No. 500. The input voltage is selected such that a displacement of ±0.375 inch produces ±5 Volts. The sensor bandwidth is 0 - 500 Hz. These sensors produce a measurement that is colocated with the control force.

2.4 Accelerometers

The structural sensors are Kistler Piezobeam accelerometers. The calibration is 10 mv/g, and have a frequency range of 0.5 to 5000 Hz. An approximate integrator is then used to integrate the acceleration signal to provide a measurement of the structural velocity[2]. The approximate integrator is given by the following input/output description

$$\frac{O}{I}(s) = \frac{\omega_c^2 s}{s^2 + \omega_c s + \omega_c^2} \tag{3}$$

This approximate integrator is the combination of a critically damped unity gain second order low pass filter, and a pure differentiator. The low pass filter provides the integrating action, while the differentiator removes the DC portion of the input signal. The transfer function is strictly proper, giving a state space realization for either analog or digital implementation. This type of integrator is used in order to avoid the integration of any DC bias produced by the accelerometer and associated signal conditioning.

2.5 Digital Controller

The digital controller used is a Systolic Systems Optima 3. The input and output voltage range is ±5 Volts The input channels are anti-alias filtered and the output channels are smooth filtered. The digital to analog converters on this system present a practical design issue, since they do not saturate. Rather, when the control law produces an output that exceeds the output range of the converter the conversion process wraps the desired signal value around the available output range. In other words, if the control law produces a desired signal of 6 Volt, the D/A converters will produce a -4 Volt signal. The solution to this problem used is to place the static controller gain on the power amplifiers. This is fine for static compensators or direct output feedback of sensor signals of known and bounded signal strength, such as the LVDT output. For dynamic compensators this is not necessarily a robust solution. A second solution would be to place logic statements in the control software that would provide saturation levels. Such logic statements would lower the achievable sampling rate.

3 Control Design

The application of a proof mass actuator to the control of a simple flexible structure is considered in this section. The structure consists of one rigid body mode, and one flexible mode of vibration. This problem is illustrated in figure 5. This problem has been proposed as a benchmark robust control problem[14]. The difference here is that the control force is produced by an actuator whose dynamics cannot be ignored. The open loop equations for this system are given by

$$\begin{bmatrix} M_S & 0 & 0 \\ 0 & M_S+m_p+m_d & m_p \\ 0 & m_p & m_p \end{bmatrix}\begin{Bmatrix} \ddot{x}1 \\ \ddot{x}2 \\ \ddot{\eta} \end{Bmatrix} + \begin{bmatrix} K_S & -K_S & 0 \\ -K_S & K_S & 0 \\ 0 & 0 & 0 \end{bmatrix}\begin{Bmatrix} x1 \\ x2 \\ \eta \end{Bmatrix} = g_{act}\begin{Bmatrix} 0 \\ 0 \\ 1 \end{Bmatrix} f_g(t) + \begin{Bmatrix} -1 \\ 1 \\ 0 \end{Bmatrix} d(t) \qquad (4)$$

The measurement equations are for the relative position, η,

$$y_p = K_{LVDT}\eta = [0\ 0\ K_{LVDT}]\ \mathbf{x} \qquad (5)$$

The following values are used for all calculations in this section.

$M_S = 1$
$0.5 < K_S < 2$, nominally $K_S = 1$
$m_p = 0.2$
$m_d = 0$
$g_{act} = 1$
$K_{LVDT} = 1$

In the following subsections several vibration control strategies are considered. The effectiveness of each system is then evaluated by giving the system an impact disturbance across masses 1 and 2, and the response of x_2 is measured. This type of disturbance does not excite the system's rigid body mode.

3.1 Controllability

The controllability of this system is then computed with standard techniques[9]

$$\text{rank}\left[B\ AB\ A^2B\ \ldots\ A^5B\right] = 4 \neq 6 \qquad (6)$$

Indicating that the system is not completely controllable. The control force produced by the actuator should be considered as a force internal to the system, and as such cannot change the location and motion of the system's center of mass. The lack of complete controllability is because the actuator cannot control the rigid body mode of the system. A further explanation of this is the actuator configured as a point force cannot produce a force at zero frequency. Therefore, a statement of the obvious is that the actuator should be only used for vibration control. In other words the actuator should be used to give the structure damping. It is also evident that a rigid body control system must be designed for this system. A design goal for the vibration control system is that it should enhance the rigid body controller.

3.2 Observability

The observability of the system is computed from

$$\text{rank}\left[C\ CA\ CA^2\ \ldots\ CA^5\right]^T = 4 \neq 6 \qquad (7)$$

Indicating that the system is also not completely observable. Similar to the previous section the rigid body modes of the system are not observable.

3.3 Vibration Absorber

The first control law considered is direct feedback of the relative proof mass position, η, and velocity, $\dot{\eta}$. This is considered a colocated design, since the resulting closed loop stiffness and damping matrices are symmetric. Although the LVDT measures the position η only, it is assumed that $\dot{\eta}$ is available from a lead network or digital derivative. This type of feedback compensation is a proportional plus derivative control. Equivalently, this type of control may also be thought of as designing an actuator spring stiffness, k_a, and viscous damper, c_a. One criterion for the choice of the feedback gains, k_a and c_a, is that used to design a passive vibration absorber[10,11,4]. The actuator spring stiffness is found from

$$\omega_a^2 = \frac{k_a}{m_p} = \frac{\omega_i^2}{(1+\mu_a)^2} \tag{8}$$

$$c_a^2 = m_p \mu_a \omega_i^2 \frac{1}{(1+\mu_a)^3} \tag{9}$$

$\mu_a = m_p(\phi_{ij})^2$
$k_a = g_{act}K_{pos}K_{LVDT}$
$c_a = g_{act}K_{vel}K_{LVDT}$
ω_i - frequency of interest, ith mode
ϕ_{ij} - jth degree of freedom, eigenvector of the ith mode, normalized with respect to the mass matrix

The resulting closed loop equations of motion are then

$$\begin{bmatrix} M_S & 0 & 0 \\ 0 & M_S+m_p+m_d & m_p \\ 0 & m_p & m_p \end{bmatrix} \begin{Bmatrix} \ddot{x}1 \\ \ddot{x}2 \\ \ddot{\eta} \end{Bmatrix} + \begin{bmatrix} 0 & 0 & 0 \\ 0 & 0 & 0 \\ 0 & 0 & c_a \end{bmatrix} \begin{Bmatrix} \dot{x}1 \\ \dot{x}2 \\ \dot{\eta} \end{Bmatrix} + \begin{bmatrix} K_S & -K_S & 0 \\ -K_S & K_S & 0 \\ 0 & 0 & k_a \end{bmatrix} \begin{Bmatrix} x1 \\ x2 \\ \eta \end{Bmatrix} = \begin{Bmatrix} -1 \\ 1 \\ 0 \end{Bmatrix} d(t) \tag{10}$$

Alternatively, the feedback gains can be calculated from the following quadratic cost function[11]

$$J = E\left[\int_0^\infty q_{ei}^2 \, dt\right] = E\left[\int_0^\infty \mathbf{z}^T \mathbf{Q} \mathbf{z} \, dt\right] \tag{11}$$

This system is stable provided that the feedback gains, k_a and c_a, are positive. The constant gain feedback of sensor signals that are colocated with an actuator does not destabilize the system. The colocation of sensors and actuators is evidenced by the symmetric closed loop stiffness and damping matrices.

The spring stiffness and damping coefficient for this example are calculated to be

$k_a = 0.331$
$c_a = 0.173$

The response of x_2 for the given disturbance is shown in figure 7. The responses shown are calculated for the minimum, maximum and nominal value for the structural spring stiffness, K_s. The vibration control system's performance when K_s is increased to its maximum value is comparable to its performance for the nominal value of K_s. On the other hand, when K_s is allowed to decrease to its minimum the performance of the system is diminished.

The performance of this type of control is explained in a control system sense as a pole-zero cancellation. The second order dynamics of the PMA add a pole and a zero to the system, which will be less that the structure's pole and zero. The zero associated with the structure will appear in between the actuator pole and the structural pole. These poles are closely spaced, since the mass ratio, μ_a, is usually small. Hence, the structural zero will tend to cancel either the actuator or the structural pole, depending on sensor and actuator placement. Because this type of control relies upon pole zero cancellation its effectiveness for more than one mode of vibration is limited.

3.4 Direct Velocity Feedback

The second control strategy considered consists of direct structural velocity feedback[13]. The idea being that the actuator will provide a force at a given point on the structure that is directly proportional and opposite in direction to the structure's velocity at that point. It is pointed that the control force is determined on the basis of both a colocated and a noncolocated sensor. Therefore, the stability of the closed loop system must be considered. The difficulty here is the design of the feedback compensator to provide the proof mass centering force. The control force is given as

$$f_g(t) = c\,\dot{x}_2 - f(\eta) \tag{12}$$

where $f(\eta)$ represents the output of the feedback compensator.

In the following subsections the velocity feedback gain, c, is held constant and two feedback compensators for η are designed. The value used for the feedback gain c is

$$c = 0.5$$

3.4.1 Direct Output Feedback

In this section a proportional plus derivative compensator is designed for the feedback of the proof mass relative position, η. Again, this type of control may be thought of as determining an equivalent actuator spring stiffness, k_a, and viscous damper, c_a. The control force is

$$f_g(t) = c\,\dot{x}_2 - k_a\eta - c_a\dot{\eta} \tag{13}$$

The closed loop equations of motion for this system are then

$$\begin{bmatrix} M_S & 0 & 0 \\ 0 & M_S+m_p & m_p \\ 0 & m_p & m_p \end{bmatrix}\begin{Bmatrix} \ddot{x}1 \\ \ddot{x}2 \\ \ddot{\eta} \end{Bmatrix} + \begin{bmatrix} 0 & 0 & 0 \\ 0 & 0 & 0 \\ 0 & -c & c_a \end{bmatrix}\begin{Bmatrix} \dot{x}1 \\ \dot{x}2 \\ \dot{\eta} \end{Bmatrix} + \begin{bmatrix} K_S & -K_S & 0 \\ -K_S & K_S & 0 \\ 0 & 0 & k_a \end{bmatrix}\begin{Bmatrix} x1 \\ x2 \\ \eta \end{Bmatrix} = \begin{Bmatrix} -1 \\ 1 \\ 0 \end{Bmatrix} d(t) \tag{14}$$

This is a noncolocated control system, and as such its stability is in question. The characteristic equation for this system is evaluated to be

$$s^2\left[s^4 + \left(\frac{c_a+c}{M_s} + \frac{c_a}{m_p}\right)s^3 + \left(\frac{2K_s+k_p}{M_s} + \frac{k_p}{m_p}\right)s^2 + \left(\frac{(c_a+c)K_s}{M_s^2} + \frac{2c_aK_s}{M_sm_p}\right)s + \left(\frac{K_sk_p}{M_s^2m_p}(2M_s + m_p)\right)\right] = 0 \qquad (15)$$

Applying the Routh-Hurwitz test to portion of the characteristic equation inside the brackets the following stability relation is obtained, assuming that each individual parameter is positive

$$\left(c_a^2 + 2c_ac + c^2\right)K_s^2m_p^2 + \left[2\left(c_a^2 + c_ac\right)K_s^2 + \left(-c_ac - c^2\right)K_sk_a\right]M_sm_p - c_acK_sk_aM_s^2 > 0 \qquad (16)$$

When the actuator damping is held at zero, i. e. $c_a = 0$, Eq.13 reduces to

$$\frac{K_s}{M_s} > \frac{k_a}{m_p} \qquad (17)$$

In other words, the actuator natural frequency should be less than the structure's natural frequency of vibration. Also, note that the velocity feedback gain, c, is not present in Eq. 14. Figure 6 illustrates the stability boundary of k_a for a range of both c_a and c, for the nominal spring stiffness K_s. Actuator spring stiffnesses below this boundary result in a stable system. The smallest stable k_a in figure 6 occurs for $c_a = 0$, independent of c. Also, the surface is relatively flat over most of the range of c_a and c, indicating that in this case stability is insensitive to actuator damping. In order to ensure stability robustness against the permissible variations in the structural spring stiffness, K_s, the minimum permitted value should be used as the nominal of design value.

The feedback gains, k_a and c_a, are determined by following the same optimization strategy that was outlined in the previous section[12]. For this example k_a and c_a are found to be

$k_a = 0.105$
$c_a = -0.0027$

The performance of this system is illustrated in figure 8. The system's settling time for both the nominal and maximum spring stiffnesses is less than that of the vibration absorber design. Although it is not apparent in this figure, when K_s is varied to its minimum value the system becomes unstable.

Following this strategy the actuator spring stiffness is found to be less than the vibration absorber spring stiffness. Performance is improved with an increased feedback gain c. In comparison to the vibration absorber system the proof mass here exhibits more relative motion and does more work on the structure.

3.4.2 Robust Control Design

An attempt to design a compensator for the feedback of the relative position, η, using an H_∞ robust control design technique was unsuccessful. The system rigid body modes were first removed from the state space equations of motion by model reduction. The rigid body mode associated with the proof mass was retained in the system equations, since it is this output that the compensator is being designed to control. The H_∞ design procedure failed because there was a plant pole on the $j\omega$-axis which then produces a closed loop pole also on the $j\omega$-axis.

3.5 Passive Damper

As a counterpoint to the above control designs the actuator is also configured to act as a passive linear damper which applies a bending moment at two locations on the structure, as shown in figure 10. Only feedback of the proof mass relative velocity, $\dot{\eta}$ is used here. In other words this is direct velocity feedback. A proof mass centering force is not required since this is provided for by the structure and fixturing. The actuator can be attached at nonadjacent joint locations to better distribute the control effort to low frequency modes.

4 Experimental Implementation

The experimental implementation of the control laws considered above is addressed in this section. An impact is given to the structure at node 1 in the x direction and the structure's acceleration is measured at node 4 also in the x direction. Each response is filtered with a 25 Hz low pass filter to give a cleaner picture of the actuator's effect. The resulting settling time for each test is used as a measure of control law performance. The actuator location is chosen in order to provide the greatest effect on the first vibration mode. The control laws are implemented digitally, with the sampling rate for each set at 4000Hz. As a basis for comparison the response of the uncontrolled structure is shown in figure 10. The settling time for this test is greater than 3.5 seconds. It is also evident that the structure must be considered more complicated than a single degree of freedom.

The vibration absorber was designed to provide damping to the first mode whose frequency is shifted to 5.8 Hz when the actuator dead mass and inertia are added. The actuator is placed at node 4. The result of this implementation is illustrated in figure 11. It is seen here that the settling time is reduced in comparison to the uncontrolled structure, but is greater than 2.5 seconds. When the actuator was tuned to the second mode at approximately 12 Hz the actuator was made unstable. This is a result of the nonlinear electromagnetic coupling of the coil and permanent magnets.

The effect of adding structural velocity feedback is shown in figure 12. The acceleration of node 4 is integrated by the approximate integrator given in Eq. 3. The cutoff frequency for the integrator is 1 Hz. Following the stability guideline for this case the actuator spring stiffness is kept low such that the actuator frequency is below that of the first mode of vibration. The settling time for this case is an improvement from the vibration absorber. Figure 12 displays a signal of approximately 1 Hz, which is the double pendulum mode of the structure suspension system. Closed loop instability for this set of feedback paths resulted when the magnitude of the disturbance impact caused the proof mass to hit the end of its stroke. These resulting impacts caused the accelerometer to overload which subsequently made the control computer overflow which induced the more proof mass impacts.

Figure 13 illustrates that the viscous damper implementation has an effect comparable to that of using structural velocity feedback. Although, there is more second mode behavior for this case. The actuator was attached at nodes 3 and 5. In comparison to the point force application of the actuator where the proof mass uses the entire stroke length, the travel of the proof mass here is at most 0.25 in.

5 Conclusions

Several structural vibration control laws have been considered analytically and implemented experimentally. Two of these control strategies are essentially active implementations of passive control concepts, namely the viscous damper and the vibration absorber. The feedback of the local structural velocity is an active control idea. A control structure interaction approach was taken in the sense that the actuator dynamics were included in the control design, and that there are several nonlinearities in the closed loop system that can lead to instability.

6 References

[1]Zimmerman, D. C., G. C. Horner, and D. J. Inman, 1988. "Microprocessor Controlled Force Actuator," *AIAA J. of Guidance, Control, and Dynamics*, Vol. 11, No. 3, pp. 230-236.

[2]Hallauer, W. and S. Lamberson, 1989. "Experimental Active Vibration Damping of a Plane Truss Using Hybrid Actuation," AIAA Paper No. 89-1169, *Proc. of the 30th AIAA/ASME/ASME/ASCE/AHS/ASC Structures, Structural Dynamics, and Materials Conference*, Mobile, AL, pp. 80-90.

[3]Balas, G. J., and J. C. Doyle, 1990. "Collocated versus Non-collocated Multivariable Control for Flexible Structure," *Proc. of the 1990 American Control Conference*, San Diego, CA, pp. 1923-1928.

[4]Minas, C., E. G. Garcia, D. J. Inman, 1989. "Control of a Flexible Planar Truss Using Proof Mass Actuators," *Proc. of the 3rd Annual Conference on Aerospace Computational Control*, Oxnard, CA, pp. 434-445.

[5]Miller, D. W. and E. F. Crawley, 1988. "Theoretical and Experimental Investigation of Space-Realizable Inertial Actuation for Passive and Active Structural Control," *AIAA J. of Guidance, Control, and Dynamics*, Vol. 11, No. 5, pp. 449-458.

[6]Balas, M. J., 1982, "Trends in Large Space Structure Control Theory: Fondest Hopes, Wildest Dreams," *IEEE Trans. on Automatic Control*, Vol. AC-27, No. 3, pp. 522-535.

[7]Hablani, H. B., 1982. "Constrained and Unconstrained Modes: Some Modeling Aspects of Flexible Spacecraft," *AIAA J. of Guidance, Control, and Dynamics*, Vol. 5, No. 2, pp. 164-173.

[8]Hughes, P. C., 1974. "Dynamics of Flexible Space Vehicles with Active Attitude Control," *Celestial Mechanics*, Vol. 9, pp 21-39.

[9]Inman, D. J., 1989. *Vibration with Control, Measurement, and Stability*, Prentice Hall, Englewood Cliffs, NJ.

[10]Den Hartog, J. P., 1956. *Mechanical Vibrations*, 4th ed., McGraw-Hill Book Co., New York, NY.

[11]Juang, J., 1984. "Optimal Design of a Passive Vibration Absorber for a Truss Beam," *AIAA J. of Guidance, Control, and Dynamics*, Vol. 7, No. 6, pp. 733-739.

12 Umland, J. W., 1989. "Proof Mass Actuators and Vibration Absorption," Mechanical Systems Laboratory Report No. 89-10, State University of New York at Buffalo, Buffalo, NY.

[13]Balas, M. J., 1979. "Direct Velocity Feedback Control of Large Space Structures," *AIAA J. Of Guidance and Control*, Vol. 2, No. 3, pp. 252-253.

[14]Wie, B., and D. S. Bernstein, 1990. "A Benchmark Problem for Robust Control Design," *Proc. of the 1990 American Control Conference*, San Diego, CA, pp. 961-962.

Mode #	Experimental Natural Frequency (Hz)	Damping Ratio (%)	MSC/PAL Natural Frequency (Hz)	Mode Type
1	6.4	0.021	6.5	1st bending
2	15.1	0.026	15.6	1st torsional
3	17.7	0.010	17.7	2nd bending
4	29.6	0.018	29.9	2nd torsional
5	35.4	0.025	35.2	3rd bending
6	45.6	0.014	45.2	3rd torsional
7	58.0	0.026	55.6	4th bending
8	63.3	0.022	60.8	4th torsional

Table 1: Modal Properties of Flexible Structure

Link O. D.	d_o	22 mm
Link I. D.	d_i	20 mm
Density	ρ	2.45×10^3 kg/m^3
Elastic modulus	E	70 GPa
Shear modulus	G	26 GPa
Joint mass	m_j	0.0759 kg
Bolt mass	m_b	0.0578 kg

Table 2: Structure link and joint characteristics

Proof mass	m_p	0.225 kg
Dead mass	m_d	0.730 kg
Dead inertia	jd	0.008 kg-m^2
Force constant	g_{act}	2.75 N/A
Friction coefficient	μ	0.01

Table 3: Linear Proof Mass Actuator Properties

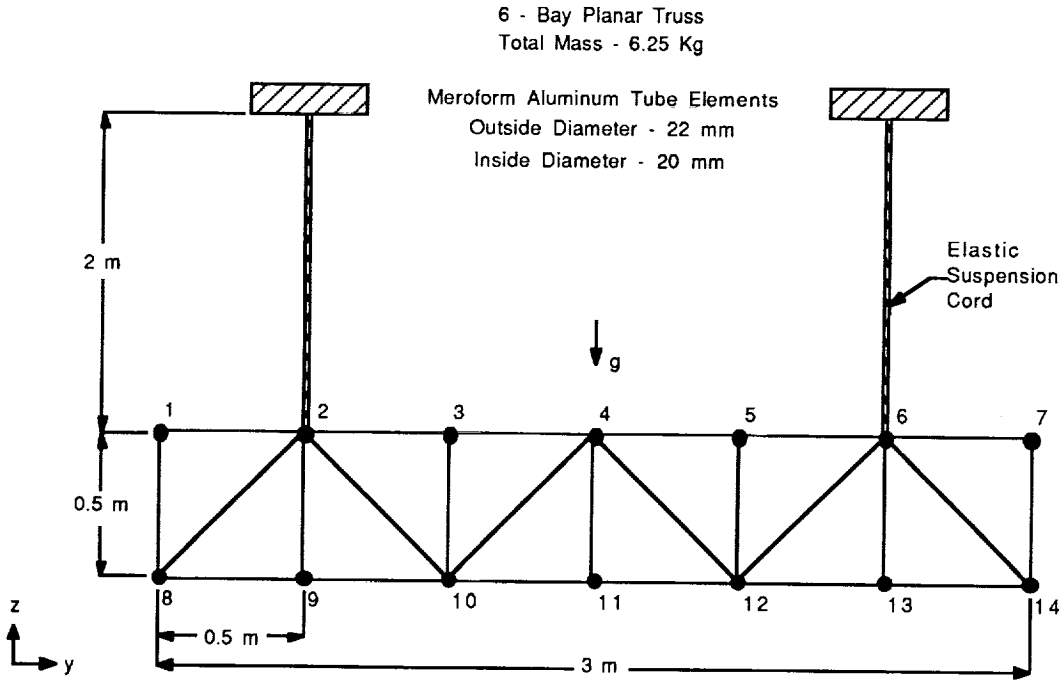

Figure 1: Experimental Flexible Structure

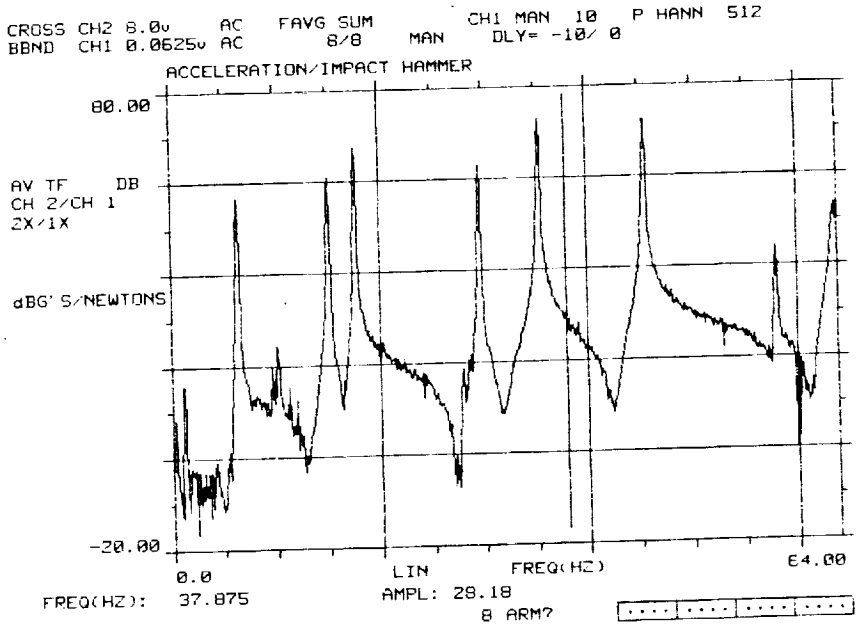

Figure 2a: Experimental Frequency Response

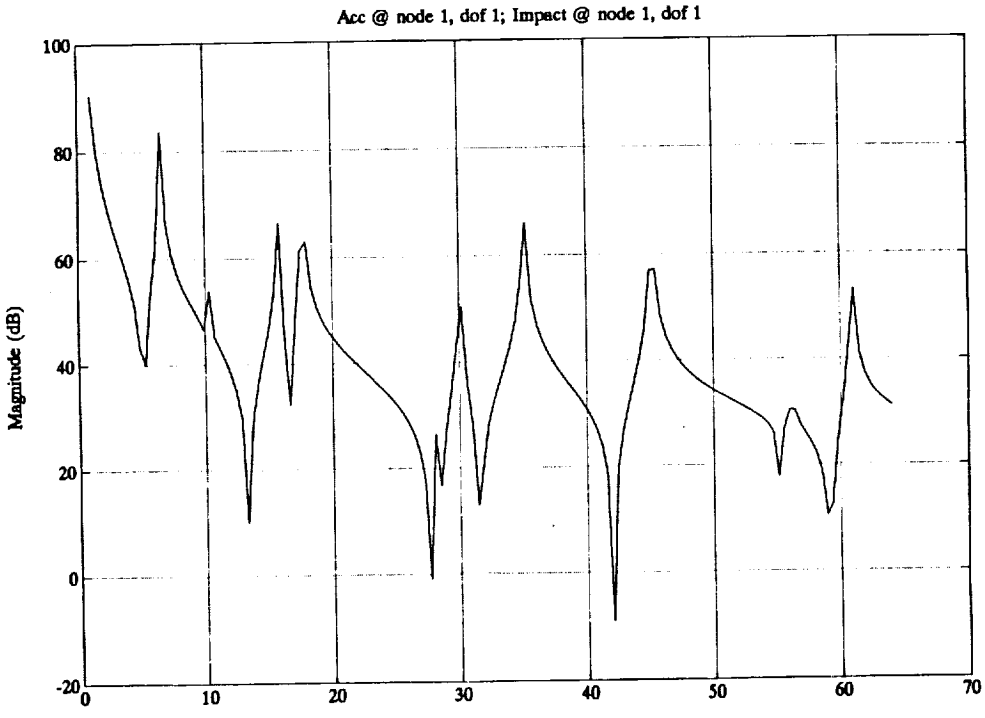

Figure 2b: Analytical Frequency Response

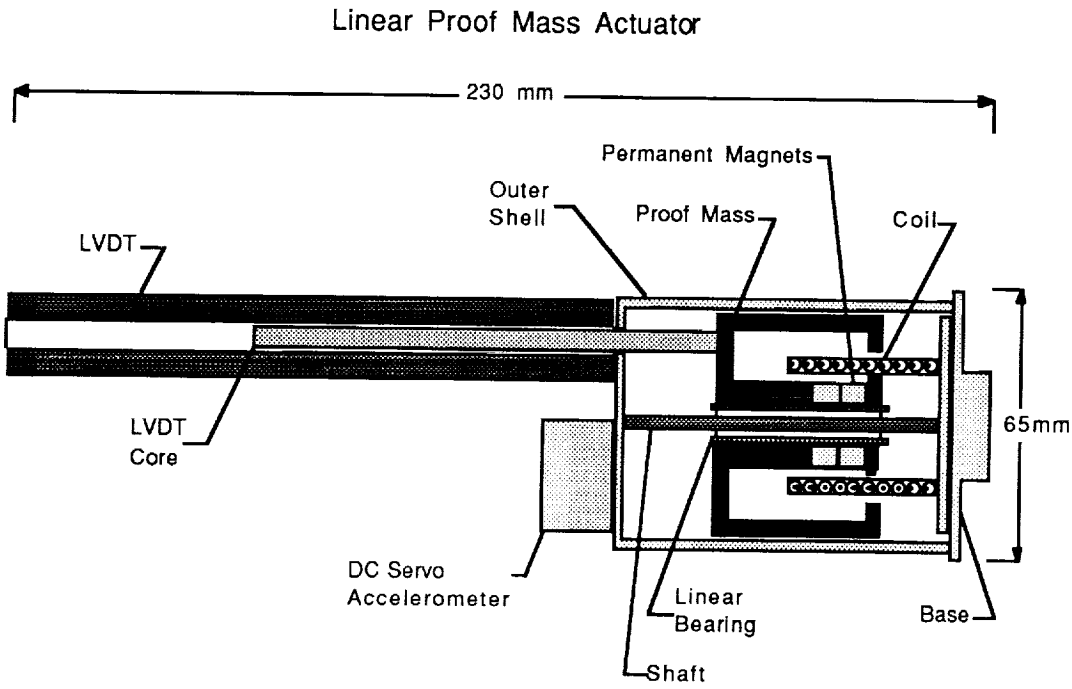

Figure 3: Linear Proof Mass Actuator

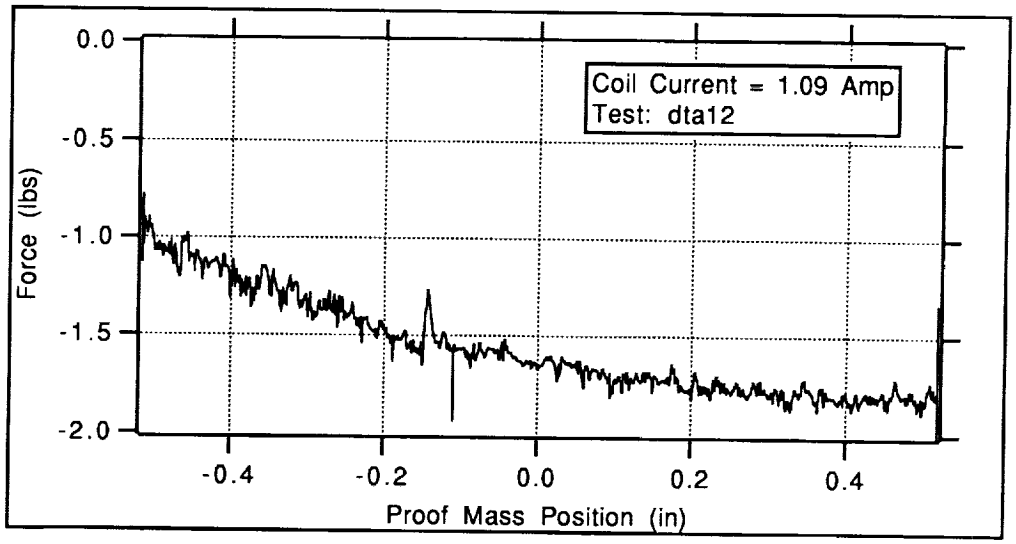

Figure 4: Static force versus proof mass position, coil current constant

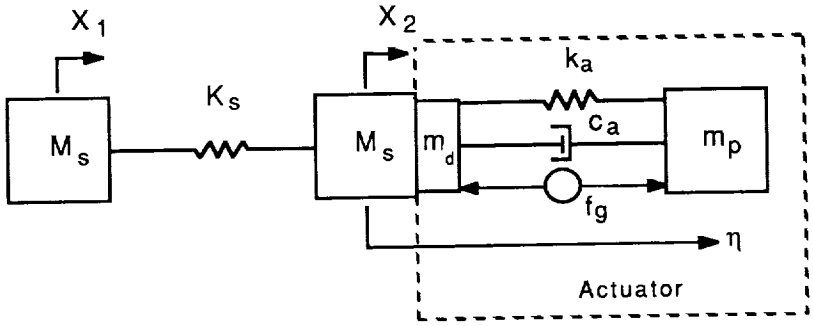

Figure 5: Free single mode structure with proof mass actuator

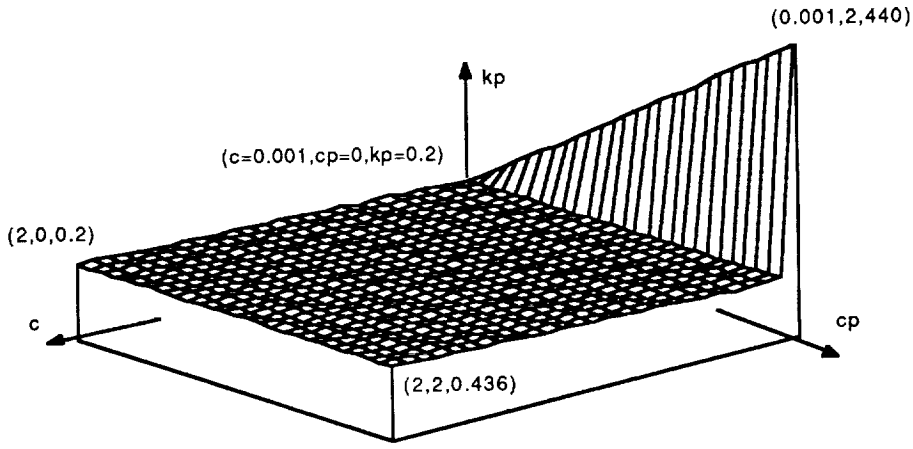

Figure 6: Constant feedback gain stability map

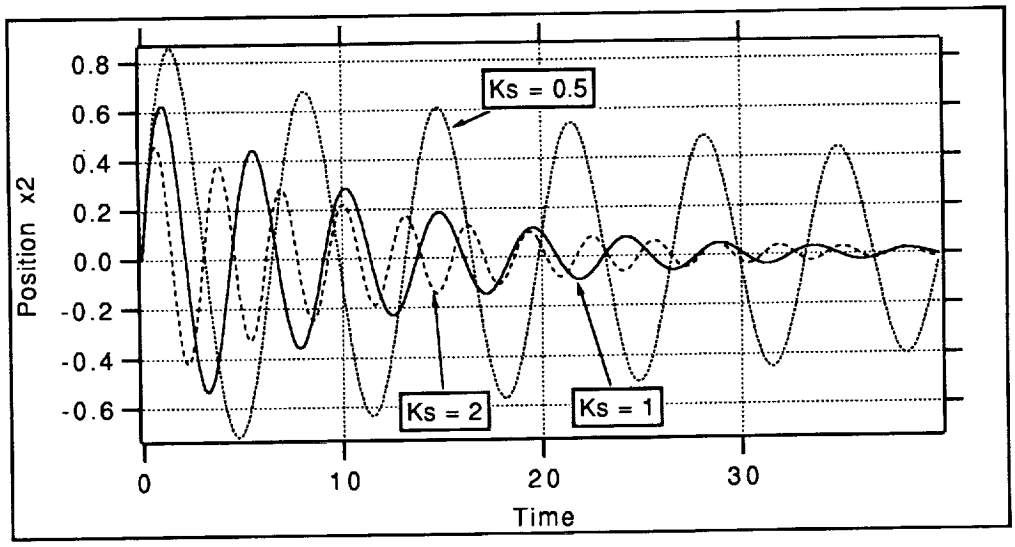

Figure 7: X_2 response to disturbance for minimum, maximum, and nominal K_s, vibration absorber design.

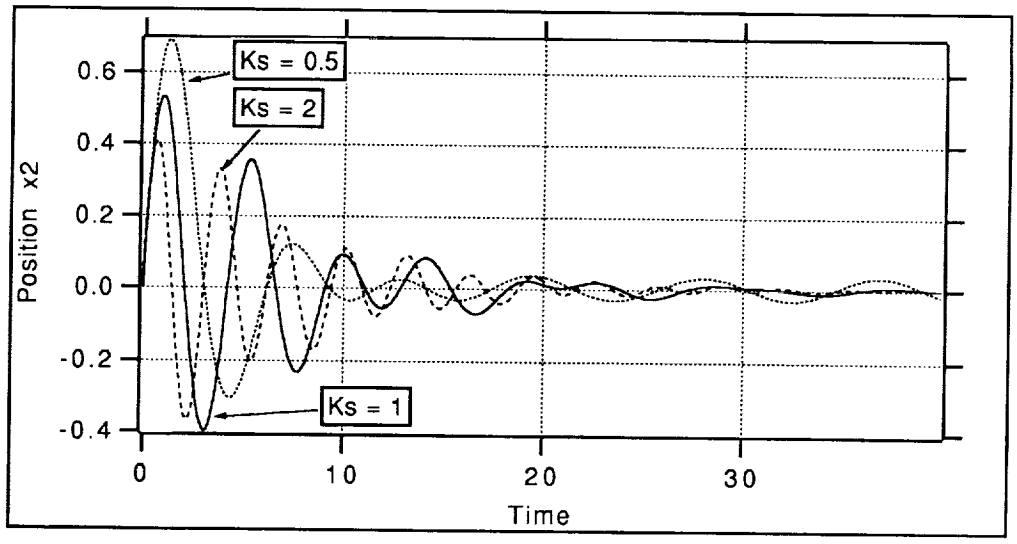

Figure 8:X2 response to disturbance for minimum, maximum, and nominal Ks, with structural velocity feedback.

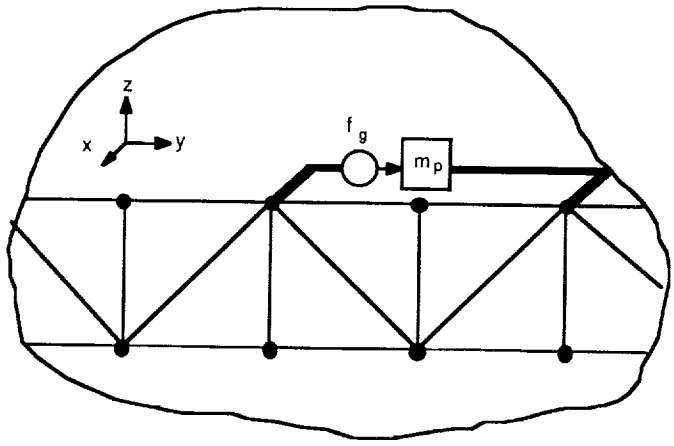

Figure 9: Viscous damper configuration.

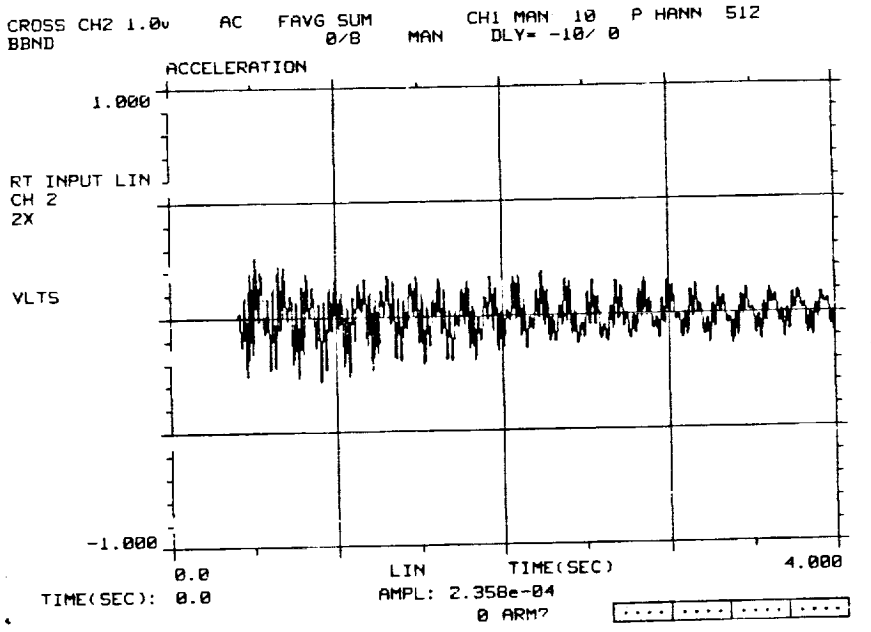

Figure 10: Response of uncontrolled structure.

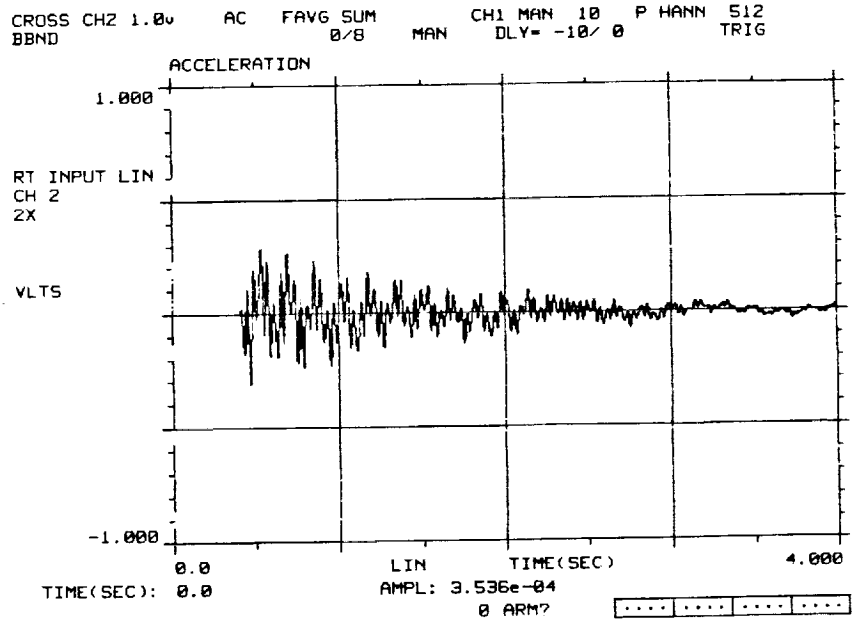

Figure 11: Response of structure, vibration absorber design.

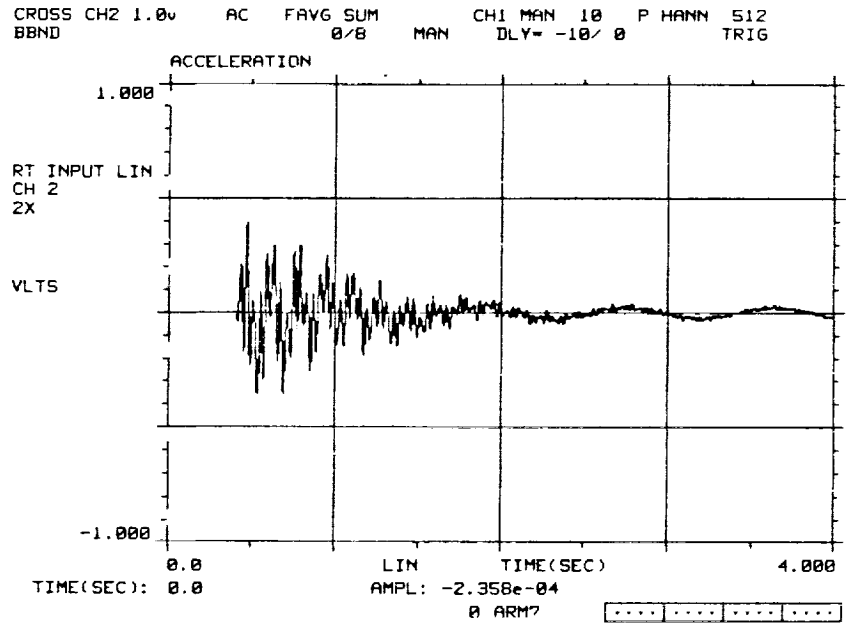

Figure 12: Response of structure, direct velocity feedback.

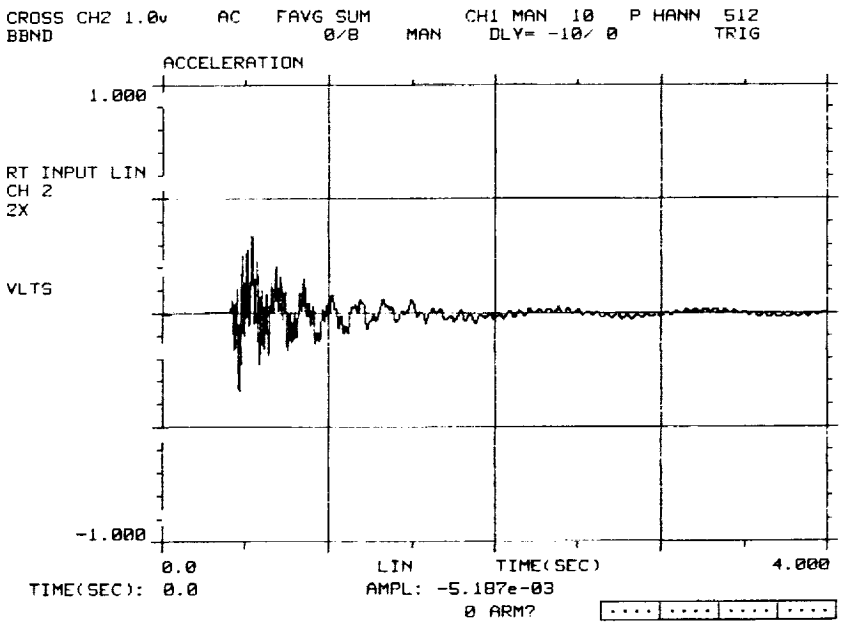

Figure 13: Response of structure, viscous damper.